Vol. 16, No. 3 (2017) 923-938
Revista Mexicana de Ingeniería Química

FLUID MOTION IN THE FLUID/POROUS MEDIUM INTER-REGION

MOVIMIENTO DE FLUIDO EN LA INTER-REGIÓN FLUIDO/MEDIO POROSO

J.A. Ochoa-Tapia[1]*, F.J. Valdés-Parada[1], B. Goyeau[2], D. Lasseux[3]
[1] *División de Ciencias Básicas e Ingeniería, Universidad Autónoma Metropolitana-Iztapalapa. Av. San Rafael Atlixco 186, col. Vicentina, 09340 Mexico, Mexico.*
[2] *Laboratoire EM2C, UPR-CNRS 288, Ecole Centrale-Supélec, Université Paris-Saclay, Grande Voie des Vignes F92-295 Châtenay-Malabry Cedex, France.*
[3] *Université de Bordeaux, I2M - TREFLE, UMR CNRS 5295, Esplanade des Arts et Métiers, 33405 Talence, Cedex, France.*
Received June 26, 2017; Accepted September 11, 2017

Abstract
In many transport and reaction processes of interest in chemical engineering, rapid velocity variations are known to take place near porous media boundaries. However, modeling the extension of the resulting boundary layers has been the subject of a long debate in the literature. In specific, modeling of momentum transport between a porous medium and a fluid has suggested the inclusion of additional terms to Darcy's law. The origin of such corrections may be regarded as a result of an upscaling method used to derive the governing equation at the Darcy scale. To address this issue, in this work we perform pore-scale simulations in an idealized porous medium model consisting in arrays of straight channels that allow obtaining analytical expressions for the Darcy-scale velocity profiles by performing an averaging (instead of an upscaling) operation. Our results show the dependence of the size and shape of transition layers with the size of the averaging domain when studying momentum transport between a porous medium and a fluid but also near the porous medium-wall boundary. With this low-computationally demanding methodology, we can conclude that the existence of an average velocity boundary layer, and thus the pertinence of correction terms to Darcy's law, is certainly justified.
Keywords: average momentum transport model, pore-scale simulations, boundary layer.

Resumen
En muchos procesos de transporte y reacción de interés en ingeniería química se sabe que ocurren variaciones rápidas de la velocidad cerca de las fronteras de medios porosos. Sin embargo, modelar la extensión de las capas límite resultantes ha sido el tema de un largo debate en la literatura. En específico, el modelado del transporte de cantidad de movimiento entre un medio poroso y un fluido ha sugerido la inclusión de términos adicionales a la ley de Darcy. El origen de tales correcciones puede verse como el resultado de un método de escalamiento para desarrollar la ecuación gobernante a la escala de Darcy. Para atender esto, en este trabajo llevamos a cabo simulaciones a escala de poro en un modelo de medio poroso idealizado que consiste en arreglos de canales rectos que permiten obtener expresiones analíticas de los perfiles de velocidad a la escala de Darcy al llevar a cabo la operación de promediado (en lugar de la operación de escalamiento). Nuestros resultados muestran la dependencia del tamaño y forma de las zonas de transición con el tamaño del dominio de promediado cuando se estudia el transporte de cantidad de movimiento entre un medio poroso y un fluido pero también en la frontera entre un medio poroso y la pared. Con esta metodología de baja demanda computacional, podemos concluir que la existencia de una capa límite de velocidad, y por tanto la pertinencia de términos de corrección a la ley de Darcy, está justificada.
Palabras clave: modelo de transporte de cantidad de movimiento promedio, simulaciones a escala de poro, capa límite.

1 Introduction

Momentum transport in the neighborhood of the fluid-porous-medium inter-region may determine the rate of heat and mass transfer in many processes of interest to chemical engineering (Whitaker, 2009). For example, this type of transport occurs in fixed bed catalytic reactors (Froment *et al.*, 2010) and many other separation systems (Wankat, 2016). Indeed, The fluid-porous medium configuration is relevant in a wide range of applications, that can go from the transport of nutrients from a fluid stream to a cellular scaffold (Yu, 2012) to forest fire modeling (Séro-Guillaume and

*Corresponding author. *E-mail*: jaot@xanum.uam.mx

Margerit, 2002), wind action over forest resulting from flow over the canopy (Wilson and Flesch, 1999; Ruck and Adams, 1991), as well as groundwater pollution modeling (Bear and Cheng, 2010), and many others. The complexity due to the porous medium structure motivates expressing the transport process in terms of average quantities, which leads to the question of representing fluid flow in the inter-region between the free fluid and the porous medium. This task may be performed by both experimental and theoretical means. In the latter case, the numerical solution of the Navier-Stokes equations in an entire porous matrix is a tremendous computational challenge.

Due to this difficulty, macroscopic momentum transport is usually modeled by the well-known Darcy's law (Bear and Cheng, 2010), which, in a vector form, may be written as,

$$\langle \mathbf{v}_\beta \rangle = -\frac{\mathbf{K}_\beta}{\mu_\beta} \cdot \left(\nabla \langle p_\beta \rangle^\beta - \rho_\beta \mathbf{g} \right) \tag{1}$$

where $\mathbf{K}_\beta$ is the porous medium intrinsic permeability tensor, whereas $\langle p_\beta \rangle^\beta$ is the intrinsic average pressure and $\langle \mathbf{v}_\beta \rangle$ is the superficial average velocity, also known as the seepage velocity (or Darcy velocity). These quantities are usually defined in terms of an averaging domain $\mathscr{V}$ (of norm V) that contains portions of the fluid and the solid phases, *i.e.*, $\mathscr{V} = \mathscr{V}_\beta + \mathscr{V}_\sigma$. Following Whitaker (1999), these quantities are defined as averages of their pore-scale counterparts by the following expressions

$$\langle p_\beta \rangle^\beta = \frac{1}{V_\beta} \int_{\mathscr{V}_\beta} p_\beta dV \tag{2a}$$

$$\langle \mathbf{v}_\beta \rangle = \frac{1}{V} \int_{\mathscr{V}_\beta} \mathbf{v}_\beta dV \tag{2b}$$

Here p_β and $\mathbf{v}_\beta$ denote the pore-scale pressure and velocity vector, respectively. The superficial and intrinsic average velocities are related by means of the Dupuit-Forchheimer relationship

$$\langle \mathbf{v}_\beta \rangle = \varepsilon_\beta \langle \mathbf{v}_\beta \rangle^\beta \tag{3}$$

with $\varepsilon_\beta = V_\beta / V$ being the porosity. Darcy's law may be regarded as a macroscopic force balance equation between the pressure gradient and the resistance offered by the porous medium. In his study of the viscous force applied by a fluid over a dense swarm of particles, Brinkman (1949) criticized Darcy's law, arguing that no viscous stress tensor has been defined in relation to it. Brinkman considered a spherical solid particle embedded in a porous medium and he required a flow expression that was valid for both high and low particle densities. Brinkman suggested to include a viscous term to Darcy's law in order to write it in the following form

$$\mathbf{0} = -\nabla \langle p_\beta \rangle^\beta + \rho_\beta \mathbf{g} + \mu_{eff} \nabla^2 \langle \mathbf{v}_\beta \rangle - \mu_\beta \mathbf{K}_\beta^{-1} \cdot \langle \mathbf{v}_\beta \rangle \tag{4}$$

where μ_{eff} is an effective viscosity coefficient, that was originally set to be equal to the fluid viscosity, μ_β, for validation purposes. An attractive feature that Brinkman found in Eq. (4) was that it reduces to Stokes' equation for conditions in which $\|\mathbf{K}_\beta\| \to \infty$ and to Darcy's law for sufficiently low values of the permeability. In this way, he was able to modify Stokes' formula to predict the permeability for systems having porosities larger than 0.6 (see Eq. (13) in Brinkman, 1949).

Motivated to provide a theoretical justification to Brinkman's model, Tam (1969) treated the swarm of particles in Brinkman's formulation as point forces in Stokes flow and performed an ensemble average, which resulted in Eq. (4). Other theoretical derivations of the Brinkman model can be attributed to Slattery (1969) and Saffman (1971), the former being carried out with the aid of the volume averaging method. Lundgren (1972), also provided a theoretical justification to Brinkman's model using ensemble averaging and found it satisfactory to take $\mu_{eff} = \mu_\beta / (1 - 5(1 - \varepsilon_\beta)/2)$ for a suspension of spheres obtaining reasonable agreement with experimental data (see Fig. 3 in Lundgren, 1972) for porosities larger than 0.6. Using the volume averaging method, Whitaker (1986) derived the Darcy-Brinkman model, which was shown to reduce to Darcy's law in the porous medium bulk. This analysis was revisited by Valdés-Parada *et al.* (2007), who concluded that, unless a slip boundary condition is considered, the effective viscosity corresponds to the fluid viscosity.

Recently, Minale (2016) derived a generalized Brinkman equation for the case of flow of a viscoelastic fluid in a porous medium using the method of volume averaging.

Certainly one of the motivations for Brinkman's modification to Darcy's law is the complication to provide boundary conditions between a porous medium and a fluid. This difficulty was circumvented by Beavers and Joseph (1967) by proposing an *ad-hoc* velocity slip boundary condition that matches Darcy's law with the Stokes' equation to model momentum transport in a channel that is partially

filled with a porous medium. This boundary condition was written in terms of an adjustable coefficient α, which ranged between 0.1 and 4 in order to match the experimental data from Beavers and Joseph (1967). However, this model cannot provide any information about the transport phenomena taking place near the fluid-porous medium surface. Certainly, the viscous term in the Brinkman model is compatible with the existence of a boundary layer, the thickness of which is estimated to be $\sqrt{\mu_{eff}||\mathbf{K}_\beta||/\mu_\beta}$ (Tam, 1969; Saffman, 1971). This motivated Neale and Nader (1974) to use the Brinkman model to study momentum transport in the porous medium and to match it with the Stokes' equations by imposing continuity conditions for both the velocity and the viscous stress. By comparing the expression of the resulting velocity profiles with the one derived by Beavers and Joseph (1967), Neale and Nader (1974) deduced that the empirical coefficient α should be equal to $\sqrt{\mu_{eff}/\mu_\beta}$. These authors recommended to use $\mu_{eff} = \mu_\beta$ until better models for the effective viscosity become available.

Ochoa-Tapia and Whitaker (1995) studied the system configuration proposed by Beavers and Joseph (1967) and deduced a momentum transport model (see Eq. (35) therein) by averaging the Stokes equations without imposing any length-scale constraints so that the average model was valid everywhere (*i.e.*, in the porous medium and in the fluid). This expression (later known as the *One-domain Approach* (ODA) by Goyeau *et al.*, 2003) is similar to Brinkman's model with three main features: 1) The effective viscosity is equal to $\mu_\beta/\varepsilon_\beta$, 2) The permeability coefficient in the Darcy term is position-dependent and 3) a second Brinkman correction term that arises by considering the porosity to be also position-dependent. Certainly, this model can be used to predict momentum transport in the whole system, including the boundary layer; however it is not a practical model to use due to the difficulties to predict the spatial variations of the effective-medium coefficients. The ODA has the attractive property that it reduces to Stokes' equation in the homogeneous fluid phase and to the Brinkman model in the porous medium (*i.e.*, the *Two-Domain Approach* (TDA), Goyeau *et al.*, 2003) by imposing appropriate constraints and assumptions as recently shown by Paéz-García *et al.* (2017). In this way, in the TDA, the upscaled models are coupled by boundary conditions, whereas in the ODA an average model is used everywhere. Ochoa-Tapia and Whitaker (1995) derived a jump in the stress and imposed continuity of the velocity as the matching boundary conditions between the Stokes and Brinkman equations, the latter being Eq. (4) with $\mu_{eff} = \mu_\beta/\varepsilon_\beta$. The key idea for the derivation of the jump conditions was the requirement that the TDA must satisfy, on average, the fields of the ODA in the zone of changes. In this way, the TDA is an approximation of the ODA and the jump condition should capture the essential transport phenomena taking place in the inter-region.

From the above, it appears that modeling momentum transport near the porous medium boundaries still holds many questions to be answered. In this context, we follow Wood (2009) who clearly made a distinction between the mathematical operation of averaging and the upscaling process. The latter implies adopting a set of length-scale constraints and assumptions with the aim of filtering out the redundant information from the microscale model and thus reducing the number of degrees of freedom involved. In the present work, rather than using this last approach, we simply average the microscale velocity profiles without making any assumption on the length-scales constraints. Since one of the main applications of upscaled models is the description of momentum transport near porous media boundaries, a fundamental question to be answered is if the transition layer is indeed a consequence of the upscaling procedure or not. This is the main purpose of this paper and in order to achieve it, we represent the porous medium as an array of straight channels that yield easy-to-handle analytical solutions. Despite the simplicity of this configuration, the analysis shows the relevant phenomena taking place near the porous medium boundaries and consequently, the conclusions reached in this work can be extended to more realistic situations in which the macroscopic flow remains one-dimensional in the direction that is parallel to the fluid-porous medium (or wall-porous medium) boundary. With this in mind, the paper is organized as follows: In Section 2 we present the microscale formulation for the system under consideration and we introduce a simplified geometry that leads to analytical solutions of the velocity profiles. These results are averaged in the different homogeneous and heterogeneous portions of the system in Section 3 in order to produce also analytical expressions for the average velocity profiles everywhere. In Section 4 we evaluate these profiles near the wall-porous medium and fluid-porous medium inter-regions in order to appreciate the resulting boundary layers and the influence of the averaging volume for different porosities. Finally, the corresponding conclusions are drawn in Section .

2 Microscale formulation

As it was mentioned before, we are interested in analyzing the fluid average velocity profile in order to demonstrate that a transition zone exists near porous media boundaries before Darcy's velocity is reached. One option to model this velocity profile could be to solve the average momentum equations that govern the fluid flow at the Darcy-scale. However, since there is no unique way to carry this out using effective-medium models, the predictions would be model-dependent. This drawback can be avoided if the average velocity profile is obtained by averaging the local velocity, which is the result of solving the pore-scale model. In a fluid-solid phase system, the local velocity of an incompressible and Newtonian fluid (the β-phase), of density ρ_β and viscosity μ_β, under steady and non-inertial flow conditions is governed by the Stokes equation

$$0 = -\nabla p_\beta + \rho_\beta \mathbf{g} + \mu_\beta \nabla^2 \mathbf{v}_\beta, \quad \text{in the } \beta\text{-phase} \tag{5a}$$

coupled to the total mass conservation equation

$$\nabla \cdot \mathbf{v}_\beta = 0, \quad \text{in the } \beta\text{-phase} \tag{5b}$$

Both equations must be solved subject to the no slip and no penetration condition at the fluid-solid interface, $\mathscr{A}_{\beta\sigma}$:

$$\mathbf{v}_\beta = \mathbf{0}, \quad \text{at } \mathscr{A}_{\beta\sigma} \tag{6}$$

along with the corresponding boundary conditions at the entrances and exits of the macroscopic system.

Since our aim is to explore the existence of the transition layers near porous media boundaries, it is convenient to consider a benchmark system as the one sketched in Fig. 1, which resembles the experimental setup used by Beavers and Joseph (1967). The system consists of a channel that is partially filled with a porous medium. The same fluid phase that saturates the porous medium flows above through the unpacked part of the horizontal channel. The seepage velocity profile can be obtained by averaging the local velocity profiles in samples like those shown in Fig. 1 that include the homogeneous (porous medium and fluid) regions and three transition zones: the wall-porous medium boundary, the porous medium-fluid boundary and the fluid-wall boundary. On the basis of the Beavers and Joseph (1967) work, it could be imposed that the flow in the upper slit and the pores is the result of the same pressure drop, *i.e.*, $(p_{inlet} - p_{outlet})/L$. From this point on, we will use the subscript η to refer to quantities associated to the homogeneous fluid phase and the subscript ω to refer to quantities related to the homogeneous porous region. In this way, L_η and L_ω denote the characteristic lengths associated to the fluid and the porous medium regions, respectively as shown in Fig. 1.

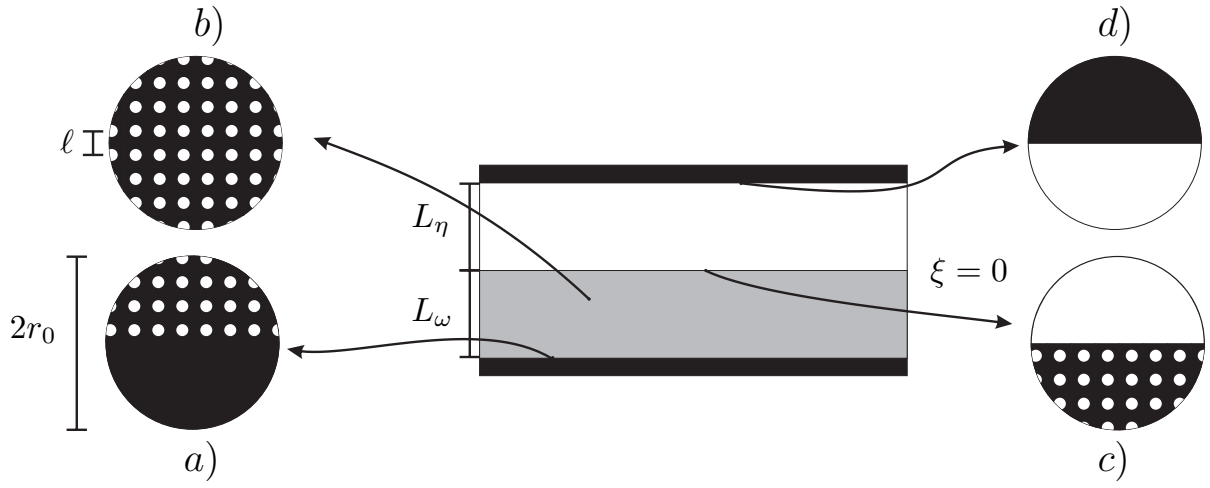

Fig. 1. Sketch of a cross-section of the system perpendicular to the flow consisting of a channel that is partially filled with a porous medium. We show the characteristic lengths of the system as well as the origin of the global coordinate system. In addition, we show samples of the averaging region at a) the wall-porous medium boundary; b) the porous medium bulk; c) the fluid-porous medium boundary and d) the fluid-wall boundary.

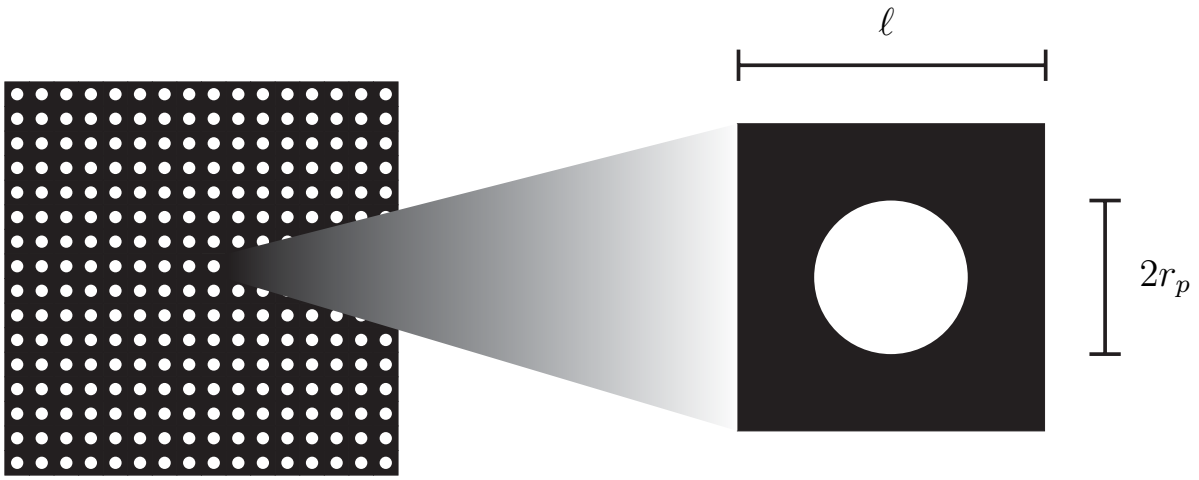

Fig. 2. View of the porous medium section perpendicular to the fluid flow direction highlighting the unit cell and its characteristic lengths.

In most cases, the solution of the pore-scale problem, due to the complexity of the fluid domain in the porous medium and fluid-solid interface, as well as the disparity of characteristic length scales (*i.e.*, $\ell \ll L_\omega$), is a tremendous computational challenge. However, it is possible to use a simplified representation of the system geometry that keeps the main characteristics of the fluid/porous medium system and for which the local velocity can be determined analytically. For example, the sample showing the porous medium bulk in Fig. 1b contains a consolidated porous medium that is formed by parallel cylindrical channels of the same diameter. At this point, it is worth stressing that the goal of this paper is not to encompass all the flow situations around the fluid-porous medium boundary, which is analytically impossible. Rather, our purpose is to provide a clear and easy to follow analysis for the classical Beavers and Joseph configuration. In this case, the analysis of a one-dimensional flow at the microscale is sufficient for our purposes. Furthermore, the analysis of experimental measurements of pointwise velocity profiles suggests that, for the Beavers and Joseph configuration, the influence of the flow in the free part of the channel is not larger than one or two unit cells inside of the porous medium (see figs. 2 and 4 in Goharzadeh *et al.*, 2005). This indicates that the value of the flow rate in the system is driven mainly due to the free channel contributions. Consequently, the size of the Brinkman layer predicted in this work should not differ, at least qualitatively, from numerical predictions or experimental measurements in more complicated geometries. Indeed, other more complicated configurations, that still yield analytical solutions, can be considered and we will discuss about them later on.

The main advantage of this porous medium configuration is that the flow in each pore and in the upper slit are only connected at the entrance and exit of the channel system. In this way, under creeping flow conditions and neglecting the effects of the vertical walls, the velocity profile of the overlaying fluid in the fully developed zone corresponds to a plane Poiseuille flow and it is given by the well-known parabolic profile expression:

$$v_z^f = v_{z,\max}^f \left[1 - \left(\frac{y_f}{B}\right)^2\right], \quad \text{for } -B \le y_f \le +B \qquad (7)$$

where $v_{z,\max}^f = (p_{inlet} - p_{outlet})B^2/2\mu L$ is the maximum velocity in the channel, B is one half of the distance between the upper wall and the porous medium interface (*i.e.*, $B = L_\eta/2$), L is the channel length and y_f is the vertical coordinate with origin at the central plane of the region (*i.e.*, $y_f = \xi - B$, where ξ is the global coordinate with origin located at the fluid-porous medium surface as shown in Fig. 1). Also, the simplicity of the system allows determining the velocity profile in each pore, which corresponds to the Hagen-Poiseuille flow equation:

$$v_z^p = v_{z,\max}^p \left[1 - \left(\frac{r}{r_p}\right)^2\right], \quad \text{for } 0 \le r \le r_p \qquad (8)$$

where $v_{z,\max}^p = (p_{inlet} - p_{outlet})r_p^2/4\mu L$ is the maximum

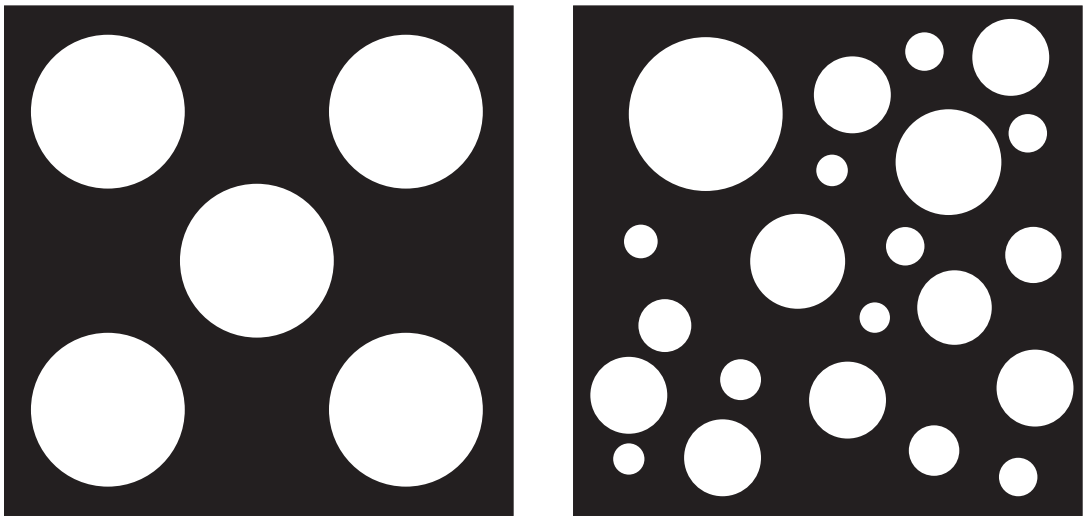

Fig. 3. Sketch of two unit cells that can be used to build the porous medium: a) a five-pore unit cell with uniform sizes and b) a random distribution of circular channels with different radii.

velocity in each pore, while r and r_p are the radial local coordinate and the radius of the pore, respectively. Furthermore, since the pressure drop, is the same for the slit and the pores, the maximum velocities are related by

$$\frac{v^p_{z,\max}}{v^f_{z,\max}} = \frac{1}{2}\left(\frac{r_p}{B}\right)^2 \tag{9}$$

The porous medium sketched in Fig. 1 could be constructed by horizontally and vertically repeating the square unit cell of side length ℓ shown in Fig. 2. It is worth emphasizing that the same velocity profile reported in Eq. (8) can be used for a porous medium with a more complex configuration like the one shown in Fig. 3a in which all the pores have the same diameter or even with a distribution of pore diameters as sketched Fig. 3b. The important issue at this point is that, after adopting a particular configuration of the consolidated porous medium, every pore can be located with reference to a global coordinate system. As a consequence, the local velocity profiles are available for the whole system, including the local velocity distribution in the upper slit. This is not easy to accomplish numerically if hundreds or thousands of pores are involved as it is required by the separation of length-scales $\ell \ll L_\omega$, which characterizes the system. The above makes evident the advantage of using the modeling approach of this work.

3 Prediction of the average velocity

The superficial average velocity is related to the local velocity by the volume averaging operator given by Eq. (2b). It is worth mentioning that this averaging operator may also be applied to the pore-scale equations (5) to obtain the average momentum equations. If no length-scale constraints or additional assumptions are applied, the resulting average equation, valid everywhere in the system, is the One-Domain Approach (Ochoa-Tapia and Whitaker, 1995) mentioned in the Introduction. Unfortunately, predictions of the permeability coefficient involved in the ODA without the imposition of length-scale constraints or assumptions are not available at the moment. For this reason, we find it more convenient to predict the average velocity directly from the pore-scale equations. It is worth recalling, that a simplified version of the ODA that involves the use of length-scale constraints leads to the Darcy-Brinkman equations as shown by Ochoa-Tapia and Whitaker (1995). It is thus interesting to find out if the transition layer results from averaging the velocity profiles without the use of any upscaling procedure.

Due to the configuration of the system shown in Fig. 1, flow can be assumed to be fully developed

not very far away from the macroscopic inlets and outlets. Hence, it is convenient to choose the averaging volume as a parallelepiped cross-sectional normal area to the flow $2r_0\ell$, where r_0 is half of the length of the averaging domain. In this way, for the upper channel, Eq. (2b) can be reduced to

$$\langle v_\beta \rangle = \frac{1}{2r_0} \int_{\xi_0 - r_0}^{\xi_0 + r_0} v_\beta(\xi)\, d\xi \tag{10}$$

where v_β is the velocity component in the horizontal direction and ξ_0 indicates the position of the centroid of the averaging domain with respect to the global coordinate system, whose origin is shown in Fig. 1.

3.1 Averaging in the fluid domain

Let us first derive the expressions of the average velocity for the regions that do not depend on the porous medium configuration. The position of the centroid of the averaging samples that contain only homogeneous fluid is restricted by

$$r_0 \le \xi_0 \le 2B - r_0 \tag{11}$$

Application of the averaging operator given in Eq. (10) to the velocity profile in the homogeneous fluid phase presented above (Eq. 7) yields

$$\frac{\langle v_\beta \rangle_\eta}{v^f_{z,\max}} = 1 - \left(\frac{\xi_0}{B} - 1\right)^2 - \frac{1}{3}\left(\frac{r_0}{B}\right)^2 \tag{12}$$

It must be noted that the above result reduces to Eq. (7) if the averaging domain is sufficiently small, *i.e.* for $r_0 \ll B$.

The other average velocity that is independent of the structure of the porous medium is the one corresponding to the upper wall/fluid transition zone (*i.e.,* the $W\eta$-inter-region). The positions of the averaging samples are restricted by

$$2B - r_0 \le \xi_0 \le 2B + r_0 \tag{13}$$

Applying once again the averaging operator, defined in Eq. (10), to Eq. (7) taking into account the fact that $v^f_z = 0$ for $\xi \ge 2B$, yields

$$\frac{\langle v_\beta \rangle_{W\eta}}{v^f_{z,\max}} = \frac{B}{2r_0}\left(\frac{2}{3} - \alpha_f + \frac{\alpha_f^3}{3}\right), \quad \alpha_f = \frac{\xi_0 - B - r_0}{B} \tag{14}$$

Note that the position of the average velocity corresponding to the solid surface in contact with the upper fluid is given by $\xi_0 = 2B$ and that the average velocity is null at this position only if $r_0 \ll B$. Otherwise the average velocity is only zero at $\xi_0 = 2B + r_0$.

3.2 Average velocity for centered pore unit cell microstructure

In this section we present expressions for the average velocity in the porous medium that are derived assuming that the pore geometry is obtained by a repetition of the simple unit cell shown in Fig. 2 in both directions orthogonal to the tube axes. Therefore, the fluid volume fraction of the homogeneous porous region, $\varepsilon_{\beta\omega}$, is related to the characteristic lengths of the microstructure by

$$\varepsilon_{\beta\omega} = \frac{\pi r_p^2}{\ell^2} \tag{15}$$

3.2.1 Average velocity in the homogeneous porous medium

For this derivation, it is convenient to choose r_0 to be an integer multiplication of the unit cell side length, ℓ, say

$$2r_0 = n_0\ell \tag{16}$$

with $n_0 \ge 1$ but in general at least larger than 10. As a consequence, for samples located in the homogeneous porous medium, Eq. (10) can be written as

$$\langle v_\beta \rangle_\omega = \frac{1}{2r_0\ell} \sum_{i=1}^{i=n_0} 2\pi \int_{r=0}^{r=r_p} v_z^p\, r dr \tag{17}$$

Substitution of Eq. (8) into the above expression and performing the corresponding integration step yields

$$\frac{\langle v_\beta \rangle_\omega}{v^p_{z,\max}} = \frac{\varepsilon_{\beta\omega}}{2} \tag{18}$$

which corresponds to the seepage velocity. The position of the centroid of the averaging domain containing only homogeneous porous medium samples is restricted by

$$-L_\omega + r_0 \le \xi_0 \le -r_0 \tag{19}$$

At this point, it is convenient to relate the size of the upper channel $L_\eta = 2B$ in terms of the size of the square unit cell side, ℓ, by

$$B = N\ell \tag{20}$$

where N is an integer number. In this way, the ratio of maximum velocities within the channel, η and in the porous region, ω given by Eq. (9), takes the form

$$\frac{v^{p}_{z,\max}}{v^{f}_{z,\max}} = \frac{\varepsilon_{\beta\omega}}{2\pi N^2} \tag{21}$$

Therefore, the average superficial velocity can be written in terms of the absolute maximum velocity of the system, which is $v^{f}_{z,\max}$, as follows:

$$\frac{\langle v_\beta\rangle_\omega}{v^{f}_{z,\max}} = \frac{\varepsilon^2_{\beta\omega}}{4\pi N^2} \tag{22}$$

3.2.2 *Average velocity at the fluid/porous inter-region, ηω*

In this transition zone, the position of the averaging volume is restricted by

$$-r_0 \le \xi_0 \le r_0 \tag{23}$$

and the samples will contain part of the homogeneous fluid, $\mathscr{V}_{\beta f}$, and part of the homogeneous porous medium, $\mathscr{V}_{\beta p}$. Therefore, Eq. (2b) can be written as

$$\langle v_\beta\rangle_{\eta\omega} = \frac{1}{V}\left(\int_{\mathscr{V}_{\beta f}} v_\beta\, dV + \int_{\mathscr{V}_{\beta p}} v_\beta\, dV\right) \tag{24}$$

Due to the particular configuration of the channel geometry, the above expression takes the form

$$\langle v_\beta\rangle_{\eta\omega} = \frac{1}{2r_0\ell}\left[\ell(\xi_0+r_0)\bar{v}^{f,\eta\omega}_z + n_p\pi r_p^2\langle v_\beta\rangle^{\beta}_{\omega} + r_p^2\phi_s\bar{v}^{p,\eta\omega}_z\right] \tag{25}$$

In this equation, the terms inside the brackets are the volumetric flow rate in the sample due to: 1) the fraction of sample that is occupied by homogeneous fluid, 2) the number of complete unit cells in the porous medium, n_p and 3) the contained fraction of the last pore (see Fig. 4b). The first of these contributions is derived by using Eq. (7) in the following definition:

$$\bar{v}^{f,\eta\omega}_z = \frac{1}{\xi_0+r_0}\int_{\xi=0}^{\xi=\xi_0+r_0} v^{f}_z(\xi)d\xi \tag{26}$$

to obtain

$$\bar{v}^{f,\eta\omega}_z = \frac{v^{f}_{z,\max}}{B}(\xi_0+r_0)\left[1-\frac{1}{3}\left(\frac{\xi_0+r_0}{B}\right)\right] \tag{27}$$

For the second contribution in Eq. (25), $\langle v_\beta\rangle^{\beta}_{\omega} = \langle v_\beta\rangle_\omega/\varepsilon_{\beta\omega}$, with $\langle v_\beta\rangle_\omega$ given by Eq. (22) and the number of complete pores, n_p, is obtained using the floor function

$$n_p = \left\lfloor -\frac{\xi_0 - r_0}{\ell}\right\rfloor \tag{28}$$

where $\lfloor x\rfloor$ returns the largest integer smaller than x.

Finally, to obtain the third flow contribution, it is necessary to determine the fraction of unit cell contained in the averaging domain, from

$$f = \frac{r_0-\xi_0}{\ell} - n_p \tag{29}$$

with the following alternatives:

1. if $f < 0.5 - r_p/\ell$, there is no contribution to Eq. (25).
2. if $f > 0.5 + r_p/\ell$, the contribution is total. This case is considered in Eq. (25) by increasing n_p by one unit and setting the third contribution to zero.
3. if $0.5 - r_p/\ell \le f < 0.5 + r_p/\ell$, the contribution is given by

$$\frac{\phi_s\bar{v}^{p,\eta\omega}_z}{v^{f}_{z,\max}} = \frac{1}{24}\left(\frac{\varepsilon_{\beta\omega}}{\pi N^2}\right)\left[3\alpha - 4\sin\alpha + \frac{1}{2}\sin(2\alpha)\right] \tag{30}$$

where

$$\alpha = 2\cos^{-1}\left[\left(\frac{1}{2}-f\right)\sqrt{\frac{\pi}{\varepsilon_{\beta\omega}}}\right] \qquad 0<\alpha<2\pi \tag{31}$$

3.2.3 *Average velocity at the porous medium/lower wall inter-region, ωW*

Finally, at the porous medium-wall transition zone (see Fig. 4a), the position of the centroid of the averaging volume is restricted by

$$-L_\omega - r_0 < \xi_0 \le -L_\omega + r_0 \tag{32}$$

In this case, the averaging volume contains part of the homogeneous porous region and the impermeable material of the lower wall occupies the rest. Therefore, the average superficial velocity is given by

$$\left\langle v_\beta\right\rangle_{\omega W} = \frac{1}{2\,r_0\ell}\left[n_p\pi\, r_p^2\left\langle v_\beta\right\rangle^{\beta}_{\omega} + r_p^2\,\phi_r\,\bar{v}^{p,\omega W}_z\right] \tag{33}$$

This result is similar to the one corresponding to the fluid/porous medium transition zone given in Eq. (25), with the exception that there is no contribution from the homogeneous fluid phase anymore.

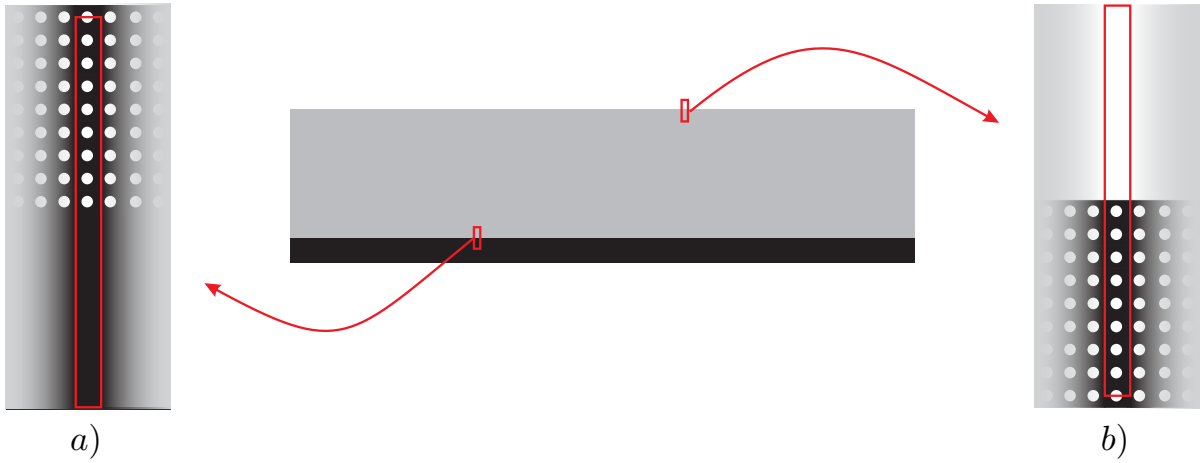

Fig. 4. Averaging volume in the porous inter-region: a) porous medium-lower wall and b) fluid-porous medium inter-region.

In addition, for the porous medium contribution, the number of complete pores, in the present case, is obtained by

$$n_p = \left\lfloor \frac{\xi_0 + L_\omega + r_0}{\ell} \right\rfloor \tag{34}$$

and the fraction of the last unit cell in the porous medium is given by

$$f = \frac{\xi_0 + L_\omega + r_0}{\ell} - n_p \tag{35}$$

Thus, the second term in the brackets of Eq. (33) can be considered in the same way as above for the cases in which $0.5 - \frac{r_p}{\ell} \leqslant f < 0.5 + \frac{r_p}{\ell}$ is not satisfied. When this inequality is satisfied, we have:

$$\phi_r \bar{v}_z^{p,\omega W} = v_{z,\max}^f \frac{\varepsilon_{\beta\omega}}{2\pi N^2} \left[\frac{\pi}{2} - \frac{1}{4}\alpha - \frac{1}{3}\sin\alpha - \frac{1}{24}\sin(2\alpha) \right] \tag{36}$$

where, in this case,

$$\alpha = 2\cos^{-1}\left[\left(f - \frac{1}{2} \right) \sqrt{\frac{\pi}{\varepsilon_{\beta\omega}}} \right] \qquad 0 < \alpha < 2\pi \tag{37}$$

3.3 *Average velocity for five pores unit cell microstructure*

To conclude this section, let us consider the unit cell shown in Fig. 3a, which incorporates five pores of the same diameter. In this case, the volume fraction is given by $\varepsilon_{\beta\omega} = 5\pi\left(\frac{r_p}{\ell}\right)^2$. In order to avoid channels overlapping, the channel radius size is restricted by the inequality $r_p \leqslant 0.5\left(\sqrt{2}-1\right)\ell$. Therefore, the maximum radius, $r_{p,\max}$, allowed is related to the unit cell size by (see Fig. 5) $\ell = 2\left(\sqrt{2}+1\right)r_{p,\max}$; and the center of each pore around the central pore is located at $\sqrt{2}r_{p,\max}$ of the symmetry axis of the unit cell.

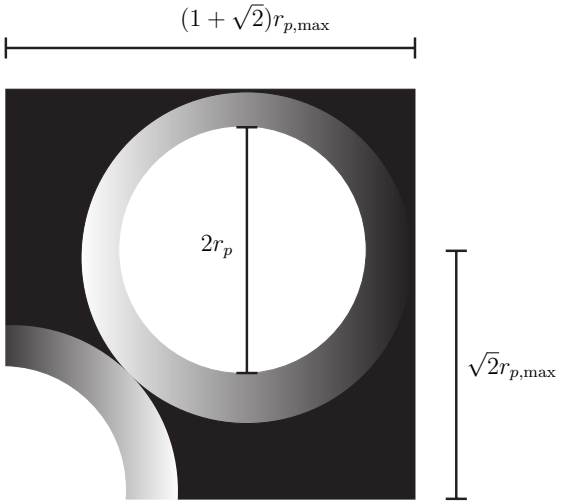

Fig. 5. Quarter of the unit cell shown in Fig. 3a including the coordinates of the centroids of the central channel and one in the upper right corner. The channel radius, r_p and its maximum value $r_{p,\max}$ are identified.

As mentioned above, the channel configuration in the porous medium does not have any effect on the average velocities in the homogeneous fluid and the upper wall/fluid inter-region, which are given by eqs.

(12) and (14), respectively. Moreover, the ratio of the maximum velocity in the slit to the one in each pore is still given by Eq. (9). However, in the present case, the average superficial velocity in the homogeneous porous medium is given by

$$\frac{\left\langle v_\beta \right\rangle_\omega}{v^f_{z,\max}} = \frac{\varepsilon^2_{\beta\omega}}{20\pi N^2} \tag{38}$$

Expressions yielding the average velocities of the two inter-regions that include a portion of the porous medium are a little more complicated than eqs. (25) and (33). However, they are obtained by the procedures outlined above and, for the sake of conciseness are not reported here although they are used for the calculations presented in the following section. Moreover, the same procedures can be used while considering unit cells with cylindrical pores of different sizes and with a much more complex distribution as the one shown in Fig. 3b. Finally, up to this point the results have been presented normalized with respect to the maximum velocity value in the homogeneous fluid phase, $v^f_{z,max}$; however, in the following section, we want to compare the velocity profiles in the different regions of the system with respect to the Darcy velocity $\langle v_\beta \rangle_\omega$. For this reason we will present the results normalized with respect to this velocity value.

4 Results and discussion

In the previous section, we derived expressions for predicting the spatial variations of the average velocity across the system, *i.e.*, from the lower to the upper walls. Briefly, the predictions of the velocity between the lower wall and the porous medium bulk (*i.e.*, from $-L_\omega - r_0 < \xi_0 \leq -L_\omega + r_0$) can be carried out using Eq. (33). The velocity in the bulk of the porous medium (*i.e.*, the Darcy velocity, $\langle v_\beta \rangle_D$) is given by Eq. (22). The use of this expression is constrained by $-L_\omega + r_0 < \xi_0 < -r_0$. The fluid-porous medium inter-region is comprised between $-r_0 \leq \xi_0 \leq r_0$ and the average velocity can be computed from Eq. (25). As mentioned above, these expressions change with the type of porous medium configuration considered in the unit cell, albeit the methodology followed to derive them remains the same. Furthermore, in the homogeneous fluid region (*i.e.*, for $r_0 \leq \xi_0 \leq 2B - r_0$), the velocity profile is predicted using Eq. (12). Finally, in the fluid-upper wall inter-region comprised between $2B - r_0 \leq \xi_0 \leq 2B + r_0$, the velocity should rapidly decrease to zero as predicted by Eq. (14). Since, in this work we model the porous medium as an array of disconnected channels with no momentum transfer between them, predictions of the average velocity in the domain $r_0 \leq \xi_0 \leq 2B + r_0$ are independent of the chosen porous medium geometry.

In order to evaluate the velocity profiles across the system, the following parameters need to be specified: i) the homogeneous porous medium porosity, $\varepsilon_{\beta\omega}$ and ii) the ratios r_0/ℓ and L_i/ℓ ($i = \omega,\eta$). In all computations we fixed $L_\omega = L_\eta = 10^5\ell$ in order to have a significant disparity of characteristic lengths between the pore-scale and the macroscale. Indeed, a smaller ratio, such as $L_\omega = 10^3\ell$ could have been used and the results were verified to be practically the same using a contrast of three or five orders of magnitude between the pore-scale and the macroscale. For the ratio r_0/ℓ, which determines the size of the averaging domain, one may choose to use a constant value of r_0 throughout the entire domain or to conveniently change its size with position and choose, for example, a large value when sampling in the porous medium (say $r_0 = \mathbf{O}(10^2\ell)$) and decrease the size of r_0 when sampling in the fluid domain. However, this approach would influence the form of the average model as explained by Cushman (2010). In the present work, we decided to use the same size of r_0 everywhere because experiments are usually carried out using the same sampling instrument in the porous medium and in the inter-region (*cf.* Goharzadeh *et al.*, 2005). At this point, it is worth recalling that the size of r_0 is not only related to the sampling instrument size but this parameter is also linked to the width of the inter-regions and thus to the limits of applications of the average models. This is a sensible issue because one may intuitively associate the positions $\xi_0 = -L_\omega$ and $\xi_0 = L_\eta$ as the points where non-slip boundary conditions must be applied macroscopically because they locate the physical system walls. As explained above, this is actually true if r_0 is sufficiently small (*i.e.*, for r_0 smaller or at most equal to ℓ); however, one should not expect the average velocity to be zero at these positions if r_0 is one or two orders of magnitude larger than ℓ.

In Fig. 6 we plot the average velocity profiles in the wall-porous medium inter-region arising from taking different sizes of the averaging domain for four values of $\varepsilon_{\beta\omega}$. Results are presented only from the location of the physical lower wall (*i.e.*, $\xi_0 = -L_\omega$) up until the end of this transition region, which is given at $\xi_0 = -L_\omega + r_0$

where the Darcy-velocity is recovered. Actually this limit value was chosen to make the average velocity dimensionless. In this way, we note that the average velocity is one half of the Darcy velocity in all cases at $\xi_0 = -L_\omega$ and it then increases in an oscillatory manner until reaching the Darcy velocity. From the results in Fig. 6 we observe that the number of oscillations, n_o is found to be equal to $r_0/\ell + 1$. Evidently, as the size of the averaging volume increases the number of oscillations becomes so large that the velocity profiles tend to a straight line. Certainly, the amplitude of the oscillations decreases as the homogeneous porous medium porosity increases thus making it easier to approach the straight line tendency. Under these conditions, it is thus not surprising that the average velocity acquires the arithmetic mean value between its bulk value and zero when the centroid is located at the physical lower wall (*i.e.*, at $\xi_0 = -L_\omega$). From the plots in Fig. 6 one can appreciate the need for the disparity of characteristic lengths between the pore-scale and the macroscale. Indeed, if one takes $L_\omega = 10^2\ell$, one may not go as high as $r_0 = 100\ell$ and recover the straight-line profile. Nevertheless, this profile is still reachable for $L_\omega = 10^3\ell$ as stated before.

From the above, it can be deduced that the size of the transition zone is directly linked to the size of the averaging volume. Moreover, it is important to remark that our intention in this work is not to provide the definitive sample size (and thus the transition layer thickness) to be used in any situation.

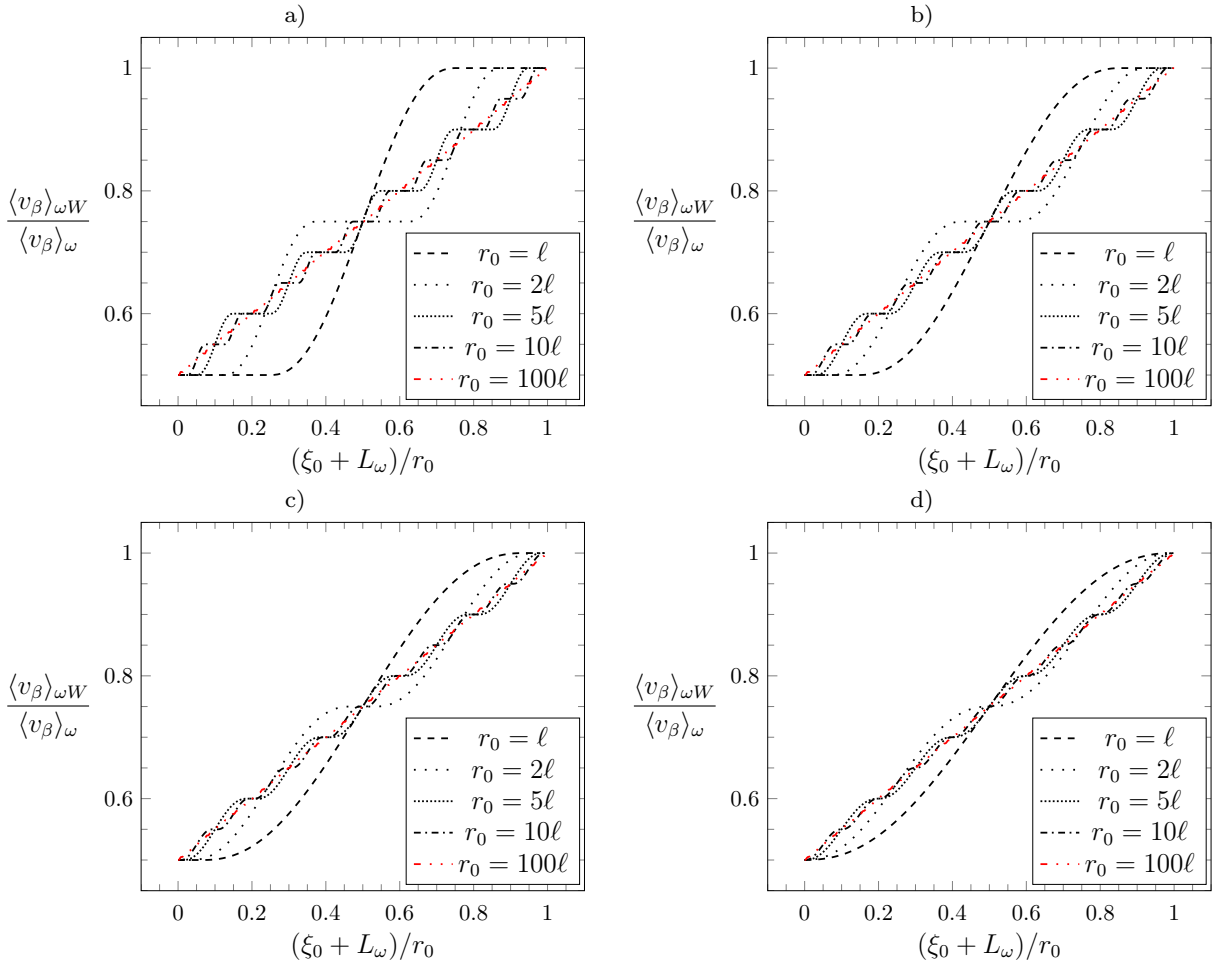

Fig. 6. Dimensionless average velocity profiles near the lower wall taking different sizes of the averaging domain r_0 for a) $\varepsilon_{\beta\omega} = 0.2$, b) $\varepsilon_{\beta\omega} = 0.4$, c) $\varepsilon_{\beta\omega} = 0.6$ and d) $\varepsilon_{\beta\omega} = 0.8$. In all the simulations we fixed $L_\eta = L_\omega = 10^5\ell$.

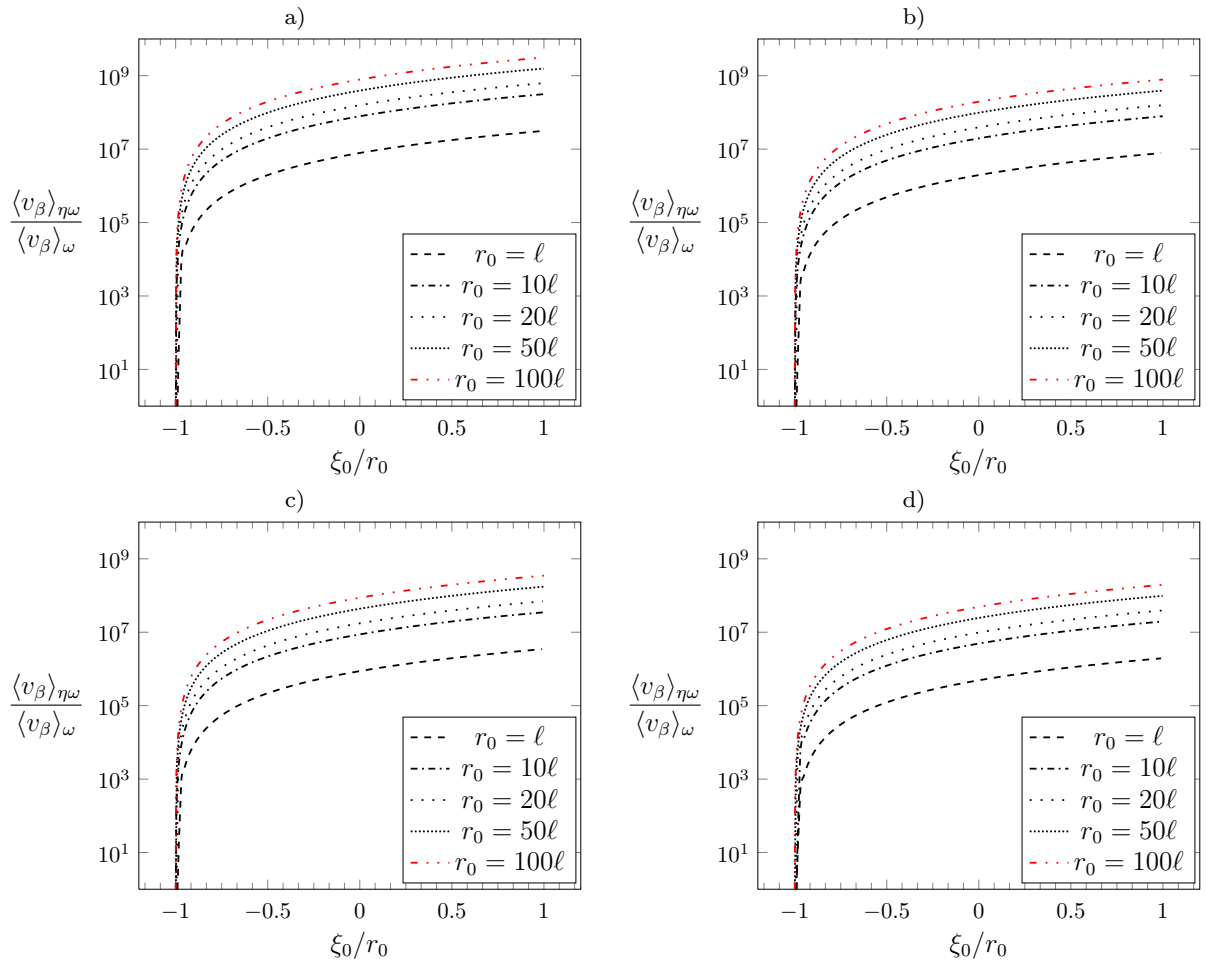

Fig. 7. Dimensionless average velocity profiles near the fluid-porous medium boundary taking different sizes of the averaging domain r_0. In all the simulations we fixed $L_\eta = L_\omega = 10^5\ell$.

Actually, in practice, the averaging size is determined according to the measuring device and the precision required in the experiment. Indeed, the averaging domain may be viewed as the response of an instrument probing intensive field variables as explained by Baveye and Sposito (1984) and Cushman (1984). In this way, the existence of a transition layer near porous media boundaries does not require a separation of scales as it is usually necessary in upscaling methods. However, the average velocity profiles depend, in general, on the size of the averaging volume as it is expected when performing experimental measurements where the results are dependent on the size of the probing device.

In the homogeneous porous medium region the velocity value is a constant that is only dependent on the porosity and the distribution of pores in the unit cell. We thus direct the attention to the velocity profiles in the fluid-porous medium inter-region shown in Fig. 7. In this case, we observe a dramatic increase of the velocity from the Darcy value to the one corresponding at the beginning of the homogeneous fluid region, which is about 8 orders of magnitude larger than the Darcy velocity. This increment is faster as the size of r_0 is increased. It is interesting to note that the existence of this transition zone is not the outcome of an upscaling procedure such as the volume averaging method or homogenization. Results shown in Fig. 7 evidence the existence of this boundary layer directly from the averaging of the pore-scale velocity profiles and it is the main contribution of this study. These remarks are applicable to all the porosity values considered here.

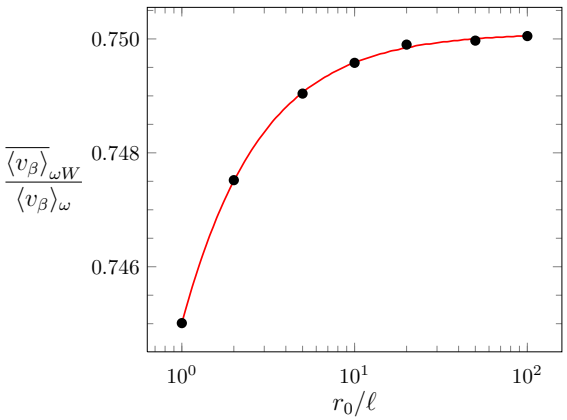

Fig. 8. Dimensionless average velocity profiles near the fluid-porous medium boundary taking different sizes of the averaging domain r_0. In all the simulations we fixed $L_\eta = L_\omega = 10^5\ell$.

For briefness in presentation, we normalized the results by presenting them in terms of $\varepsilon^2\langle v_\beta\rangle_{\eta\omega}/\langle v_\beta\rangle_\omega$ instead of plotting the average velocity in the fluid-porous medium transition layer for each porosity value. Interestingly, under this form, the shape of these velocity profiles resembles the one exhibited by the experimental results reported in Fig. 6b by Morad and Khalili (2009). The results shown in figures 6 and 7 clearly show that there is a slip velocity when the centroid of the averaging domain is located at the physical lower wall and when it is located at the surface of the last channel in contact with the fluid.

In addition, we performed simulations considering the five-pore unit cell depicted in Fig. 3a as well as using parallel plates as a porous medium model (*i.e.*, a plane Poiseuille-flow model). In both situations we obtained qualitatively the same velocity profiles as those shown in figs. 6 and 7 for $r_0 < 100\ell$ and quantitatively the same values for $r_0 \geq 100\ell$. Finally, the velocity profiles in the homogeneous fluid region are independent to the averaging volume size and of the type of porous medium under consideration and, for the sake of brevity, are not presented here.

To conclude this section, it is appropriate to redirect the attention to the wall-porous medium inter-region and suggest a methodology for choosing an appropriate value for r_0. As a particular criterion, one may take the average of the velocity profiles in the inter-region (say $\overline{\langle v_\beta\rangle}_{\omega W}$) for each value of r_0/ℓ and choose the value of r_0 that leads to closer predictions to an asymptotic value of the average velocity. An example of the application of this criterion is shown in Fig. 8, which corresponds to the averages of the data presented in Fig. 6a) along with a statistical fit that was obtained by means of a logistic equation. In this case we found that, for $r_0 = 20\ell$, the relative error percent with respect to the asymptotic value was less than 0.01%, whereas for $r_0 = 100\ell$ the value of the error percent is reduced in one order of magnitude. We performed tests for the other velocity profiles shown in Fig. 6 obtaining similar results. This criterion for choosing the averaging volume size should be relevant for carrying out numerical simulations to predict the spatial variations of effective medium coefficients, present in upscaled models, that take place in the wall-porous medium inter-region but should also shed some light about the size of the sampling device that should be used to collect experimental data in that region. Nevertheless, these observations should be taken with care because the weighting function for the intrinsic averages is taken here to be the inverse of the rectangular function of the fluid within the averaging domain, while in practice this weighting function could be more complicated.

Conclusions

In this work we studied momentum transport near porous media boundaries in an idealized system resembling the classical one proposed by Beavers and Joseph (1967). In specific, the fundamental question that motivated this work is whether or not the existence of transition layers is the result of an upscaling process. With this in mind, we proposed an idealized model for the porous medium geometry consisting of arrays of channels that yield analytical solutions for the pore-scale velocity profiles. While spatially smoothing (*i.e.*, averaging) the pore-scale velocity fields we obtained velocity profiles at the Darcy scale that evidenced the existence of transitions layers as shown in figs. 6 and 7. From these results, it is clear that the existence and size of these layers (either between a porous medium and a wall or a porous medium and a fluid) is directly related to the averaging volume size, r_0. Before moving on, it is worth recalling that the latter conclusion was reached in a simplified system that did not allow momentum exchange between the porous medium and the fluid. More than a limitation, this choice of geometry is a point of emphasis, because it indicates that, given that a sufficiently large averaging domain exists, boundary layers in this type of systems are the result of an averaging process. In our computations we took the

modeling choice of fixing the averaging volume size to be the same regardless of the centroid position; hence once an r_0 value is chosen so are the widths of the transition layers. Interestingly, boundary layers appear even for cases in which r_0 is equal to the unit cell size ℓ, which is the minimum value of r_0 required to recover the seepage velocity. As expected, when r_0 is *sufficiently large* with respect to ℓ (*i.e.*, $r_0 = \mathbf{O}(10^2\ell)$), the Darcy velocity predictions at the porous-medium/wall boundary tend to a single profile, which is the same when using other configurations for the pores in the unit cell.

Although the porous medium configuration is certainly idealized and does not allow pore-scale momentum exchange between the porous medium and the adjacent fluid, the fact that it yields analytical predictions of the pore-scale and Darcy-scale velocities is encouraging because of the minimal computational cost that implies simulating the entire system. As a matter of fact, the numerical solution of the pore-scale equations in a system with the disparity of characteristic lengths involved in figs. 6 and 7 is a tremendous computational challenge and may only be addressed in an approximate manner. Furthermore, in dispersed porous media it is well known that the effect of the upper free flow motion on the local velocity reaches the depth of two or three particles. However the effect on the average velocity will be of the same order of magnitude as the one found in the present study. The minimum size of the sample will correspond to one unit cell and even in such a case a transition layer will exist. A much larger sample may be required due to changes in the micro structure or to experimental needs. For this reason, simulations performed here, although approximate, provide a qualitative idea of the spatial variations of the velocity near porous media boundaries. It should be stressed that, for situations in which many transport processes take place, such as convective heat transfer in porous media, the approach used in this work is not that simple and additional criteria are needed in order to define the thickness of the transition layer. Nevertheless, our approach may be used for example to study diffusive mass transfer between a porous medium and a fluid or between different porous media.

Finally, as a matter of prospective, the analysis presented here may be used to predict the spatial variations of effective-medium terms and coefficients involved in the one-domain approach. In other words, the transport phenomena taking place in the transition layers may not necessarily be completely captured only by the Brinkman correction term; instead other correction terms (involved in the one-domain approach) are necessary. Indeed, as explained by Valdés-Parada *et al.* (2013) this information is necessary for the closure process involved in jump boundary conditions.

Acknowledgments This work was benefited from Fondo Sectorial de Investigación para la educación from CONACyT (Project number: 256231).

Nomenclature

$\mathscr{A}_{\beta\sigma}$	solid-fluid interface
B	half of the width of the upper channel, m
f	fraction of a unit cell
$\mathbf{g}$	gravity acceleration vector, m/s^2
$\mathbf{K}_\beta$	permeability tensor, m^2
ℓ	size of the unit cell side, m
L	channel length, m
L_i	width of the i-region ($i = \omega,\eta$), m
n_0	number of unit cells contained by the averaging volume
n_p	number of unit cells in the averaging volume that are contained in the porous medium
N	number of unit cells in half of the width of the upper channel
p_β	pore-scale pressure, Pa
p_i	($i = inlet$) inlet or ($o = outlet$) outlet pressure, Pa
$\langle p_\beta\rangle^\beta$	intrinsic average pressure, Pa
r	radial local coordinate normal to axis of each pore direction, m
r_p	radius of each pore, m
r_0	half of the characteristic length size of the averaging volume, m
$\mathbf{v}_\beta$	pore-scale velocity vector, m/s
v_z^i	axial component of the velocity vector in the channel ($i = f$) or in each pore ($i = p$), m/s
$v_{z,\max}^i$	maximum velocity in the channel ($i = f$) or in each pore ($i = p$), m/s
$\langle\mathbf{v}_\beta\rangle$	superficial average velocity vector, m/s
$\mathscr{V}$	averaging domain of norm V
$\mathscr{V}_\beta$	domain occupied by the β-phase within $\mathscr{V}$
y_f	local coordinate normal to the axial direction in the middle of the upper channel, m

Greek symbols

α	angle that defines fraction of pore that contributes to flow

ε_β fluid volume fraction
μ_β fluid dynamic viscosity, Pa·s
μ_{eff} effective viscosity, Pa·s
ρ_β fluid density, kg/m^3
ξ coordinate normal to the flow direction whose origin is located at the interface between the upper fluid and the first solid of the porous medium, m

Subscripts
β refers to the β-phase
η refers to the homogeneous fluid region
$\eta\omega$ refers to the homogeneous fluid/porous medium inter-region
ω refers to the homogeneous porous medium region
ωW refers to the homogeneous porous medium/lower wall inter-region
$W\eta$ refers to upper wall/homogeneous fluid inter-region

Superscripts
f refers to the upper channel fluid
p refers to the pore fluid

References

Baveye, P. and Sposito, G. (1984). The operational significance of the continuum hypothesis in the theory of water movement through soils and aquifers. *Water Resources Research 20*, 521–530. doi:10.1029/wr020i005p00521.

Bear, J. and Cheng, A. (2010). *Modeling Groundwater Flow and Contaminant Transport*. Springer. doi:10.1007/978-1-4020-6682-5.

Beavers, G. and Joseph, D. (1967). Boundary conditions at a naturally permeable wall. *Journal of Fluid Mechanics 30*, 197-207. doi:10.1017/s0022112067001375.

Brinkman, H. (1949). A calculation of the viscous force exerted by a flowing fluid on a dense swarm of particles. *Applied Scientific Research A1*, 27-34. doi:10.1007/bf02120313.

Cushman, J. (1984). On unifying the concepts of scale, instrumentation, and stochastics in the development of multiphase transport theory. *Water Resources Research 20*, 1668–1676. doi:10.1029/wr020i011p01668.

Cushman, J. (2010). *The Physics of Fluids in Hierarchical Porous Media: Angstroms to Miles*. Springer. doi:10.1007/978-94-015-8849-2.

Froment, G., Bischoff, K. and Wilde, J. D. (2010). *Chemical Reactor Analysis and Design*, volume 26. Wiley, third edition. doi:10.1002/aic.690260330.

Goharzadeh, A., Khalili, A. and Jorgensen, B. (2005). Transition layer thickness at a fluid-porous interface. *Physics of Fluids 17*, 057102. doi:10.1063/1.1894796.

Goyeau, B., Lhuillier, D., Gobin, D. and Velarde, M. (2003). Momentum transport at a fluid-porous interface. *International Journal of Heat and Mass Transfer 46*, 4071–4081. doi:10.1016/s0017-9310(03)00241-2.

Lundgren, T. (1972). Slow flow through stationary random beds and suspensions of spheres. *Journal of Fluid Mechanics 51*, 273-299. doi:10.1017/s002211207200120x.

Minale, M. (2016). Modelling the flow of a second order fluid through and over a porous medium using the volume averages. I. the generalized Brinkman's equation. *Physics of Fluids 28*, 023102. doi:10.1063/1.4941575.

Morad, M. and Khalili, A. (2009). Transition layer thickness in a fluid-porous medium of multi-sized spherical beads. *Experiments in Fluids 46*, 323–330. doi:10.1007/s00348-008-0562-9.

Neale, G. and Nader, W. (1974). Practical significance of Brinkman's extension of Darcy's law: coupled parallel flows within a channel and a bounding porous medium. *Canadian Journal of Chemical Engineering 52*, 475–478. doi:10.1002/cjce.5450520407.

Ochoa-Tapia, J. and Whitaker, S. (1995). Momentum transfer at the boundary between a porous medium and a homogeneous fluid. I Theorical development. *International Journal of Heat and Mass Transfer 38*, 2635–2646. doi:10.1016/0017-9310(94)00346-W.

Paéz-García, C. T., Valdés-Parada, F. J. and Lasseux, D. (2017). Macroscopic momentum and mechanical energy equations for incompressible single-phase flow in porous media. *Physical Review E 95*, 023101. doi:10.1103/physreve.95.023101.

Ruck, B. and Adams, E. (1991). Fluid mechanical aspects of the pollutant transport to coniferous trees. *Boundary Layer Meteorology 56*, 163–195. doi: 10.1007/bf00119966.

Saffman, P. (1971). On the boundary condition at the surface of a porous medium. *Studies in Applied Mathematics 50*, 93-101. doi:10.1002/ sapm197150293.

Séro-Guillaume, O. and Margerit, J. (2002). Modelling forest fires. Part I: A complete set of equations derived by extended irreversible thermodynamics. *International Journal of Heat and Mass Transfer 45*, 1705–1722. doi: 10.1016/s0017-9310(01)00248-4.

Slattery, J. (1969). Single-phase flow through porous media. *AIChE Journal 15*, 866–872. doi:10.1002/ aic.690150613.

Tam, C. (1969). The drag on a cloud of spherical particles in low Reynolds number flow. *Journal of Fluid Mechanics 38*, 537-546. doi:10.1017/ s0022112069000322.

Valdés-Parada, F., Aguilar-Madera, C., Ochoa-Tapia, J. and Goyeau, B. (2013). Velocity and stress jump conditions between a porous medium and a fluid. *Advances in Water Resources 62*, 327–339. doi: 10.1016/j.advwatres.2013.08.008.

Valdés-Parada, F. J., Ochoa-Tapia, J. A. and Alvarez-Ramirez, J. (2007). On the effective viscosity for the Darcy-Brinkman equation. *Physica A: Statistical Mechanics and its Applications 385*, 69–79. doi: 10.1016/j.physa.2007.06.012.

Wankat, P. C. (2016). *Separation Process Engineering*. Prentice Hall. ISBN 0133443655.

Whitaker, S. (1986). Flow in porous media I: A theoretical derivation of Darcy's law. *Transport in Porous Media 1*, 3–25. doi:10.1007/bf01036523.

Whitaker, S. (1999). *The Method of Volume Averaging*. Kluwer Academic Publishers. doi: 10.1007/978-94-017-3389-2.

Whitaker, S. (2009). Chemical engineering education: Making connections at interfaces. *Revista Mexicana de Ingeniería Química 8*, 1–33.

Wilson, J. and Flesch, T. (1999). Wind and remnant tree sway in forest cutblocks. III. A wind flow model to diagnose spatial variation. *Agricultural and Forest Meteorology 93*, 259–282. doi:10.1016/ s0168-1923(98)00121-x.

Wood, B. (2009). The role of scaling laws in upscaling. *Advances in Water Resources 32*, 723–736. doi:10.1016/j.advwatres.2008.08.015.

Yu, P. (2012). Numerical simulation on oxygen transfer in a porous scaffold for animal cell culture. *International Journal of Heat and Mass Transfer 55*, 4043–4052. doi:10.1016/j.ijheatmasstransfer. 2012.03.046.